Int. J. Heat Mass Transfer. Vol. 30, No. 1, pp. 69 84, 1987
Printed in Great Britain

0017-9310/87 $3.00+0.00
Pergamon Journals Ltd.

Heat transfer and friction in the offset strip-fin heat exchanger

HIMANSHU M. JOSHI* and RALPH L. WEBB†

* Pennsylvania State University, Behrend College, Erie, PA 16563, U.S.A.
† Department of Mechanical Engineering, Pennsylvania State University, University Park, PA 16802, U.S.A.

(*Received* 7 *October* 1985 *and in final form* 24 *April* 1986)

Abstract—This paper presents analytical models to predict the heat transfer coefficient and the friction factor of the offset strip-fin heat exchanger surface geometry. Two flow regimes are defined—laminar and turbulent. Based on the conditions in the wake, an equation is developed to predict transition from laminar to turbulent flow. Flow visualization experiments were performed to identify the flow structure at transition. The condition predicted by the transition equation corresponds to onset of oscillating velocities in the fin wakes. Equations are developed for the Nusselt number and friction factor by writing energy and momentum balances on a unit cell of the offset strip-fin geometry. A numerical solution is used to calculate Nu and f on the fins in the laminar regime, and a semi-empirical approach is used for the turbulent regime. Predictions are compared to data on scaled-up geometries, taken in the present study, and data on actual heat exchangers. The models predict all data within $\pm 20\%$.

INTRODUCTION

THE OFFSET strip-fin is a commonly used geometry in plate-and-fin heat exchangers. These exchangers are characterized by high heat transfer area per unit volume, and high heat transfer coefficients. A view of the offset strip-fin geometry is shown in Fig. 1. Heat transfer enhancement is obtained by periodic growth of laminar boundary layers on the fin length (l), and their dissipation in the fin wakes. This enhancement is accompanied by an increase in pressure drop because of increased friction factor. A form drag force, due to the finite thickness of the fins, also contributes to the pressure drop. The geometry of the offset strip-fin is defined by the four dimensions h, l, s and t, or the three dimensionless parameters $\alpha = s/h$, $\delta = t/l$ and $\gamma = t/s$. It is assumed that the fins are offset uniformly, by half the fin spacing, as can be seen in Fig. 1.

Over forty years of research has been done on the offset strip-fin geometry. It includes data on actual heat exchangers and scaled-up models [1–8], flow visualization experiments [8–12], analytical models [13], empirical correlations [14–16], and numerical solutions [17–19]. The analytical model of Kays [13] treats the fins as short, flat plates in laminar flow. Comparison of the predictions of the model to data shows only fair agreement. The numerical solutions of refs. [17, 18] are based on the assumption of zero-thickness fins. The solution of Patankar and Prakash [19] is for finite thickness fins, but its validity has not been established by comparison with data. All three numerical solutions assume laminar wakes throughout the range of interest of flow rates. However, flow visualization studies of Mochizuki and Yagi [12] have shown that, in the range of interest, the wake velocities begin to oscillate. At some higher flow rate, vortices are shed from the fins and are swept over the laminar boundary layers. Thus the numerical solutions are valid only for the laminar wake condition. As reported by Shah and Webb [20], the state-of-the-art for predicting the j and f characteristics of the offset strip-fin, are the empirical correlations of Wieting [15]. These correlations consist of power-law curve fits of the j and f values for 22 heat exchanger surface geometries as functions of Re_D and the dimensionless geometric parameters l/D_h, α and t/D_h. These correlations have no theoretical basis and should not be used outside the ranges of the geometries of the surfaces used to develop the correlations.

Two practical considerations, not addressed in previous theoretical models, are the effects of burred fin ends and the roughness on the top and bottom walls of the offset strip-fin channel. Burred fin ends are

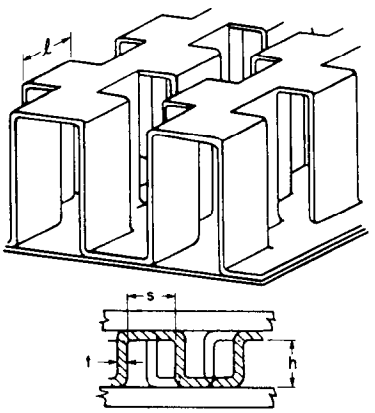

FIG. 1. Geometry of the offset strip-fin.

† To whom correspondence should be addressed.

NOMENCLATURE

A_f	frontal area of unit cell
b	defined by equation (2)
C_D	drag coefficient
D_h	hydraulic diameter for the offset strip-fin channel, equation (7)
D'_h	hydraulic diameter for a rectangular channel, equation (13)
f	average friction factor in the offset strip-fin array
f_p	average friction factor on the fin sides
f_e	average friction factor on the top and bottom walls
h	height of the offset strip-fin channel
h_B, h_F	average heat transfer coefficient on the back and front ends of the fins
h_e	average heat transfer coefficient on the top and bottom walls
h_o	overall average heat transfer coefficient
h_p	average heat transfer coefficient on the fin sides
j	$Nu/Re_D Pr^{1/3}$
j_e	$Nu_e/Re_{sh} Pr^{1/3}$
j_p	$Nu_p/Re_D Pr^{1/3}$
k	thermal conductivity of fluid
l	fin length
l_s^+	$(l/2s)/Re_s$
Nu	average overall Nusselt number, $h_o D_h/k$
Nu_e	average Nusselt number on the top and bottom walls, $h_e D'_h/k$
Nu_p	average Nusselt number on the fin sides, $h_p 2s/k$
ΔP	pressure drop
Pr	Prandtl number of fluid
Re	Reynolds number, $Re_D = \rho v D_h/\mu$, $Re_{sh} = \rho u D'_h/\mu$, $Re_t = \rho v t/\mu$, $Re_l = \rho v l/\mu$, $Re_b = \rho v b/\mu$
s	spacing between adjacent fins
t	fin thickness
u	velocity based on flow area sh
v	velocity based on flow area $(s-t)h$.

Greek symbols

α	aspect ratio s/h
δ	t/l
γ	t/s
τ_p	shear stress on the fin sides
τ_e	shear stress on the top and bottom walls
ρ	density of fluid
μ	viscosity of fluid
η	overall surface efficiency
η_f	fin efficiency.

caused by the shearing process used in their manufacture, and the roughness results from bending continuous metal strips into rectangular Z-shapes. This roughness may be seen in Fig. 1. Burred fin ends cause an effective increase in fin thickness and, therefore in the form drag. They may also lead to leading-edge separation. The top and bottom surface roughness may cause an increase in both heat transfer and friction.

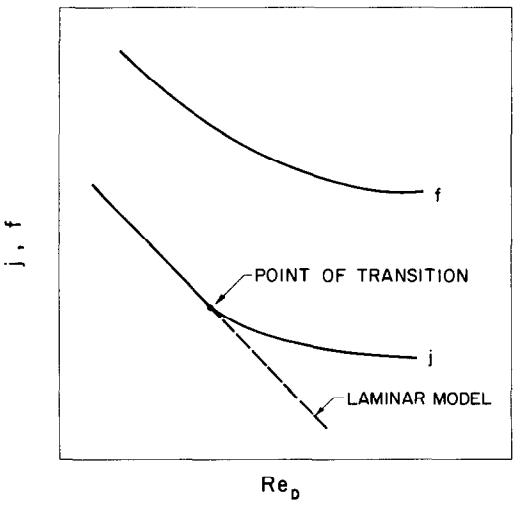

FIG. 2. Typical j and f characteristics.

The present study had three objectives:

(1) To define a criterion for transition from laminar boundary layers and laminar wakes. Flow rates smaller than that at transition are classified as laminar and those higher are classified as turbulent.
(2) To develop analytical models to predict the heat transfer and friction characteristics in the laminar and turbulent flow regimes.
(3) To obtain accurate friction factor data on scaled-up, precisely dimensioned geometries, and conduct flow visualization studies on scaled-up arrays to relate the flow structure in the wake to the transition criterion described earlier.

TRANSITION IN THE WAKES

Flow visualization studies of two collinear plates [9, 10] and of fin arrays [8–12] have shown that, as the flow rate is increased, the wakes develop oscillating velocities. These oscillating velocities affect the transport of energy and momentum in the boundary layers on the fins, although the boundary layers are still laminar. The change in the wake flow affects the j and f characteristics as seen in a typical j and f vs Re_D plot, shown in Fig. 2. At small values of Re_D, the wakes are laminar, and a laminar model is applicable for prediction of the j and f values. As Re_D increases, the j

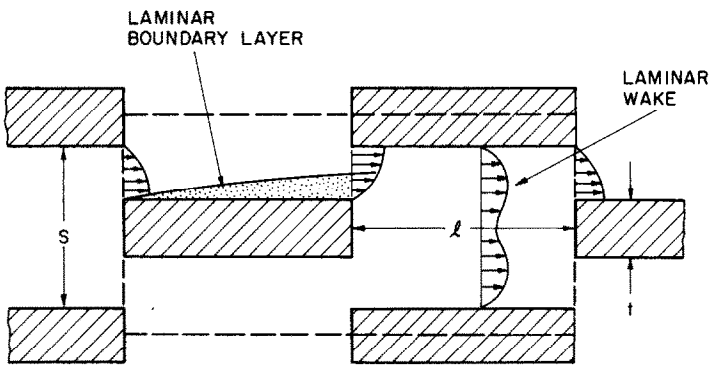

FIG. 3. Laminar flow on the fins and in the wakes.

and f curves change slopes and the laminar model will then underpredict the data. The change of slope occurs over a small Re_D range. In this study, the value of Re_D at which the curves begin to deviate from the straight laminar line is defined as the 'point of transition'. It is denoted by Re_D^*. The region $Re_D < Re_D^*$ is the laminar region. The character of the flow on the fins and in the wakes of the laminar condition is illustrated in Fig. 3. The region $Re_D > Re_D^*$ is the turbulent region. This flow condition is shown in Fig. 4. In the turbulent region, the boundary layers on the fins are still laminar. This was confirmed during the flow visualization tests that are described later. Also, plate fin heat exchangers typically operate at $200 < Re_D < 4000$. At $Re_D = 4000$, the value of Re_l may be as high as 24,000 (for $l/D_h = 6$), compared to $Re_l = 500{,}000$ at which transition to turbulence occurs on a flat plate. Therefore, the change in the slope of the j and f curves must be caused by changes in the wake flow structure and their effects on the downstream boundary layers. A criterion to predict the changes in the wakes will be developed.

Previous studies of the wake region have not studied the effect of the fin length (l), the fin thickness (t), and the fin spacing (s) on the wake flow pattern. The flow visualization part of this study was designed to study these variations.

The correlation to predict the point of transition for any given offset strip-fin geometry was obtained from the data of 21 heat exchangers from refs. [3–5]. Their geometries are shown in Table 1. The procedure is described below.

The Reynolds numbers Re_D^* corresponding to the slope changes of the j and f curves are visually read from the plots of the data. These are converted to wake width based Reynolds numbers Re_b^* using

$$Re_b^* = Re_D^* \times \frac{b}{D_h} \tag{1}$$

$$b = t + 1.328l/(Re_l)^{0.5} \tag{2}$$

$$D_h = \frac{2(s-t)h}{(s+h)+ht/l}. \tag{3}$$

In equation (2), b is the wake width defined as the fin thickness plus twice the momentum thickness at the trailing-edge of the fin. The hydraulic diameter (D_h) is defined using the minimum cross-sectional area in the channel and the total heat transfer area.

The characteristic of the flow in the wake is its velocity profile. It is affected by the spacing between the fins (s). The width of the wake, as defined by equation (2) is a function of the fin thickness (t) and the fin length (l). To account for these effects, the Re_b^* values obtained from equation (1) were correlated with the nondimensional parameters t/l and l/s. A

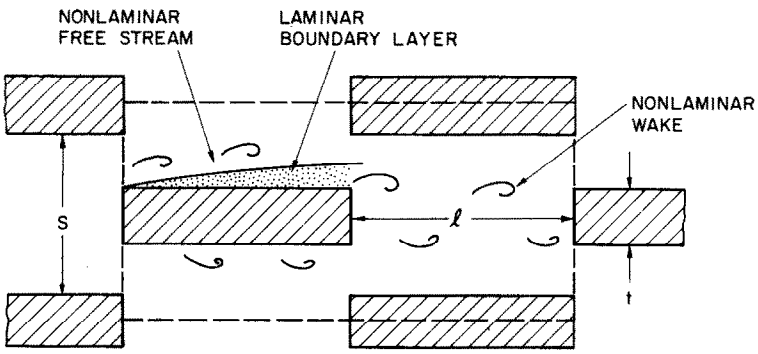

FIG. 4. Laminar flow on the fins and oscillating flow in the wakes.

Table 1. Geometric parameters of 21 heat exchanger cores

No.	Ref.	Fig. in ref.	Symbol*	D_h (mm)	α (s/h)	δ (t/l)	γ (t/s)
1	3	10–60	□	1.255	0.134	0.040	0.121
2	3	10–57	○	1.562	0.135	0.036	0.100
3	3	10–63	△	3.124	0.161	0.043	0.051
4	3	10–58	+	1.334	0.184	0.036	0.111
5	3	10–55	×	2.230	0.244	0.032	0.067
6	3	10–67	◇	1.961	0.410	0.028	0.067
7	3	10–66	↑	2.537	0.461	0.023	0.051
8	3	10–68	⋈	1.681	0.477	0.048	0.106
9	3	10–70	Z	1.422	0.487	0.032	0.086
10	3	10–56	Y	1.402	0.489	0.032	0.081
11	3	10–71	□	1.400	0.492	0.032	0.081
12	3	10–59	◆	1.087	0.528	0.036	0.107
13	3	10–72	×	1.552	0.593	0.048	0.107
14	3	10–69	★	1.549	0.597	0.048	0.107
15	3	10–65	⊕	1.631	0.628	0.024	0.102
16	3	10–61	⊖	1.295	0.670	0.040	0.084
17	4	5–3 (28R)	↓	0.693	0.675	0.060	0.202
18	3	10–64	ω	2.121	0.712	0.012	0.077
19	3	10–62	α	1.176	1.0	0.020	0.041
20	5	10	δ	0.632	1.0	0.020	0.038
21	4	5–3 (20R)	ε	0.937	1.0	0.060	0.136

* Symbols are used in Figs. 13, 15, 16 and 17. See Appendix for definitions of D_h.

power law expression was obtained, using multiple regression

$$Re_b^* = 257(l/s)^{1.23}(t/l)^{0.58}. \quad (4)$$

Table 2 shows the Re_D^* values read from the data, the corresponding Re_b^* values for the j slope change, and the value of Re_b^* predicted by equation (4). The Re_D^* values at the j and f slope changes are equal within the error of observation, but the j values were chosen to calculate Re_b^* because the change in slopes of the j curves were observed to be sharper and more readily identifiable. Equation (4) correlates the observed Re_b^* values with an r.m.s. deviation of 14%. The relationship between Re_b^* and the flow pattern at this Re_b^* will be established later.

ANALYTICAL MODELS

Definitions

The analytical models to predict the j and f factors are developed by writing an energy and a momentum balance on the unit cell shown in Fig. 5. In the offset

Table 2. Reynolds numbers at transition

Surface No. from Table 1	Re_D at j slope change	Re_D at f slope change	Re_b at j slope change	Re_b^* equation (4)	Re_b^*/Re_b
1	1100	1000	152	154	1.01
2	900	900	110	130	1.18
3	—	800	—	51	—
4	1300	800	177	148	0.84
5	900	900	95	86	0.91
6	800	600	97	93	0.97
7	700	600	76	76	1.00
8	700	600	115	116	1.01
9	700	600	101	116	1.16
10	1000	1000	146	108	0.74
11	700	700	103	109	1.05
12	800	700	135	142	1.05
13	600	600	107	118	1.10
14	600	800	107	118	1.10
15	900	900	156	174	1.11
16	900	700	145	98	0.68
17	—	—	—	222	—
18	1100	1100	169	192	1.14
19	700	700	80	64	0.80
20	400	400	54	58	1.08
21	—	—	—	136	—

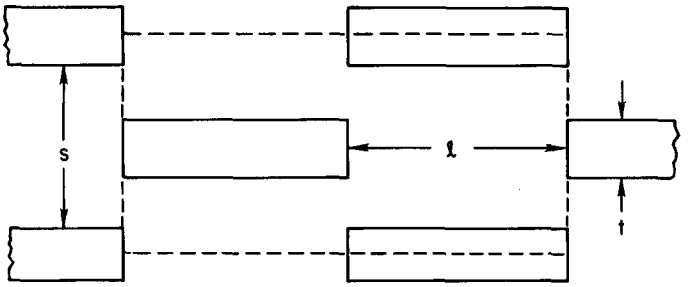

FIG. 5. Unit cell used in the analytical models.

strip-fin array, the velocity and temperature profiles become fully developed in the periodic sense, at some length downstream from the entrance. That is, they repeat from fin to fin. This means that the non-dimensional profiles are identical at corresponding positions on successive fins. The unit cell of Fig. 5 is chosen such that it lies in this region. In Fig. 5, h is the dimension perpendicular to the plane of the paper. This unit cell is an idealization of the actual geometry because it neglects the possible burrs on the fin ends and also the roughness on the top and bottom of the channel. For Fig. 5, the hydraulic diameter D_h is defined as

$$D_h = \frac{4 \times \text{minimum flow area}}{\text{heat transfer area per unit length}}. \quad (5)$$

Thus

$$D_h = \frac{4(s-t)h/2}{(lh+th+ls)/l} = \frac{2(s-t)h}{(s+h)+ht/l}. \quad (6)$$

In terms of the three dimensionless parameters, D_h is

$$D_h = \frac{2s(1-\gamma)}{(1+\alpha+\delta)}. \quad (7)$$

The Reynolds number in the channel is defined as

$$Re = \frac{\rho v D_h}{\mu} \quad (8)$$

where v is the maximum velocity in the channel—based on the cross-sectional area $(s-t)h$.

Heat transfer

In steady-state flow, an energy balance on the unit cell gives

$$4(lh+th+ls)\eta h_o = 4lh\eta_f h_p + 4th\eta_f(h_B+h_F) + 4lsh_e \quad (9)$$

where

h_p is the average heat transfer coefficient on the fin sides

h_e is the average heat transfer coefficient on the top and bottom walls

h_B, h_F are the average heat transfer coefficients on the back and front ends of the fin

h_o is the average overall heat transfer coefficient

η_f is the fin efficiency

η is the overall surface efficiency, defined as $\eta = 1-[1-(A_{fin}/A)]\eta_f$ where A_{fin} = surface area of the fins and A = surface area of the base plus the fins.

It is reasonable to use the approximation $h_p = h_B = h_F$. The fin ends typically contain about 5% of the total surface area. A preliminary calculation shows that a 50% error in the estimate of h_B and h_F would result in a 5% error in h_o. Rewriting equation (9) in terms of α, δ and γ, and solving for ηh_o gives

$$\eta h_o = \frac{(1+\delta)}{(1+\alpha+\delta)}\eta_f h_p + \frac{1}{(1/\alpha+\delta/\alpha+1)}h_e. \quad (10)$$

Expressing the heat transfer coefficients in dimensionless form as Nusselt numbers

$Nu = h_o D_h/k$ the average overall Nusselt number

$Nu_p = h_p 2s/k$ the average Nusselt number on the fin sides (11)

$Nu_e = h_e D'_h/k$ the average Nusselt number on the top and bottom walls.

Equation (10) becomes

$$\eta Nu = \frac{1+\delta}{(1+\alpha+\delta)}\frac{D_h}{2s}\eta_f Nu_p + \frac{1}{(1/\alpha+\delta/\alpha+1)}\frac{D_h}{D'_h}Nu_e \quad (12)$$

where D'_h is the hydraulic diameter of a rectangular channel of cross-section $s \cdot h$, and is defined as

$$D'_h = \frac{4sh}{2(s+h)} = \frac{2s}{(1+\alpha)}. \quad (13)$$

Using equations (6) and (13) in equation (12)

$$\eta Nu = \frac{(1-\gamma)}{(1+\alpha+\delta)}\left[\frac{1+\delta}{(1+\alpha+\delta)}\eta_f Nu_p + \frac{(1+\alpha)}{(1+1/\alpha+\delta/\alpha)}Nu_e\right]. \quad (14)$$

Equation (14) is used to calculate the heat transfer coefficient of the offset strip-fin channel. The completion of the model requires a theoretical basis to predict Nu_p and Nu_e. Separate models are used for the laminar and turbulent flow regions.

Friction factor

A force–momentum balance on the unit cell of Fig. 5 is used to derive an equation for the friction factor. Since the unit cell is in the periodic fully developed flow region, the net rate of change of momentum, and hence the net force on the unit cell is zero. So

$$\Delta P A_f - \tau_p 4lh - \tau_e 4ls - C_D \tfrac{1}{2}\rho v^2 \left(\frac{4t}{2} h\right) = 0. \quad (15)$$

The first term represents the force due to the pressure gradient, the second and third terms are the shear forces on the fin sides and the top and bottom walls, and the last term is the drag force due to the finite fin thickness.

A_f is the frontal area of the unit cell
τ_p is the shear stress on the fin sides
τ_e is the shear stress on the top and bottom walls
C_D is the form drag coefficient.

Define the following friction factors

$$f = \frac{\Delta P}{\frac{1}{2}\rho v^2} \times \frac{D_h}{4(2l)} \quad \text{(composite value for the array)}$$

$$f_p = \frac{\tau_p}{\frac{1}{2}\rho v^2} \quad \text{(on fin sides)} \quad (16)$$

$$f_e = \frac{\tau_e}{\frac{1}{2}\rho v^2} \quad \text{(on top and bottom walls).}$$

Using the above friction factor definitions in equation (15), one obtains

$$\frac{\Delta P}{\frac{1}{2}\rho v^2} \times \frac{D_h}{4(2l)} \times A_f \times \frac{4(2l)}{D_h} \times \frac{1}{4lh} = \frac{\tau_p}{\frac{1}{2}\rho v^2} + \frac{\tau_e}{\frac{1}{2}\rho v^2} \frac{s}{h} + C_D \frac{t}{2l} \quad (17)$$

which may be solved for f to yield

$$f \frac{2A_f}{D_h h} = f_p + \alpha f_e + C_D \frac{t}{2l}. \quad (18)$$

Using $A_f = h(s + t)$, and equation (7), in equation (17)

$$f = \frac{1-\gamma}{(1+\alpha+\delta)(1+\gamma)} (f_p + \alpha f_e + C_D t/2l). \quad (19)$$

This is the final expression for the average overall friction factor in the unit cell of Fig. 5. Now one must establish methods to predict f_p, f_e and C_D, for the laminar and turbulent regimes.

Laminar models

The laminar flow model applies when $Re_b < Re_b^*$. The component Nusselt numbers and friction factors, and C_D are predicted as explained below.

Prediction of Nu_p and f_p. Sparrow and Liu [18] have numerically predicted Nu_p and f_p for the case of $\alpha = \delta = \gamma = 0$. A zero aspect ratio ($\alpha = 0$) corresponds to the condition $s \ll h$. The present model uses a curve fit of the Sparrow and Liu values for $\alpha = \delta = \gamma = 0$, and develops correction factors that apply when α, δ and γ are non-zero. Sparrow and Liu present tabled values of Nu_p and f_p as a function of the entrance length parameter (l_s^+), where

$$l_s^+ = (l/2s)/Re_s \quad (20)$$

$$Re_s = \rho u 2s/\mu \quad (21)$$

and u is the velocity in the channel based on the cross-sectional area ($s \cdot h$). A curve fit of their tabled values gives the following expressions.

$$Nu_s = 24.2 - 3692(l_s^+) - 0.37 \times 10^6 (l_s^+)^2 \quad (22)$$

$$f_s = [262 - 46{,}537(l_s^+) + 0.535 \times 10^7 (l_s^+)^2]/4Re_s. \quad (23)$$

As noted previously, the present model assumes $h_B = h_F = h_P$.

Since equations (22) and (23) are for $\alpha = 0$, it is necessary to correct them for the case of $\alpha > 0$. The following correction factors are employed

$$\frac{Nu_p}{Nu_s} = \frac{Nu_{EL\alpha}}{Nu_{EL0}} \quad (24)$$

$$\frac{f_p}{f_s} = \frac{f_{EL\alpha}}{f_{EL0}}. \quad (25)$$

The subscripts EL0 and ELα indicate the entrance length values for rectangular channels of aspect ratios zero and α, respectively. The corrections $Nu_{EL\alpha}/Nu_{EL0}$ and $f_{EL\alpha}/f_{EL0}$ are plotted as functions of l_s^+ with α as a parameter, in Fig. 6. The entrance length solutions are taken from Shah and London [21].

Prediction of Nu_e and f_e. The ideal unit cell shown by Fig. 5 has smooth top and bottom walls. The model assumes that Nu_e and f_e may be predicted using solutions for laminar, fully developed flow in a rectangular channel. That is, it is assumed that the fins do not affect the boundary layers on the top and bottom surfaces. Shah and London [21] provide these values in tabular form and as fifth degree polynomials. Simpler third degree polynomials were developed by the authors, assuming a constant wall temperature boundary condition

$$Nu_e = 7.45 - 16.9\alpha + 22.1\alpha^2 - 9.75\alpha^3 \quad (26)$$

$$f_e = (23.94 - 30.05\alpha + 32.37\alpha^2 - 12.08\alpha^3)/Re_{sh} \quad (27)$$

where

$$Re_{sh} \equiv Re_D/B \quad (28)$$

and

$$B \equiv \frac{1+\alpha}{1+\alpha+\delta}. \quad (29)$$

Thus, the RHS of equations (24) and (25) are read from Fig. 6.

The drag coefficient (C_D). For finite fin thickness, $\delta > 0$, the pressure difference on the up and downstream blunt faces results in a form drag. Kays [13] used $C_D = 0.88$ in his approximate model. This results from the solution for potential flow [22] normal to a long, thin plate, assuming the pressure in the wake is equal to the free-stream value.

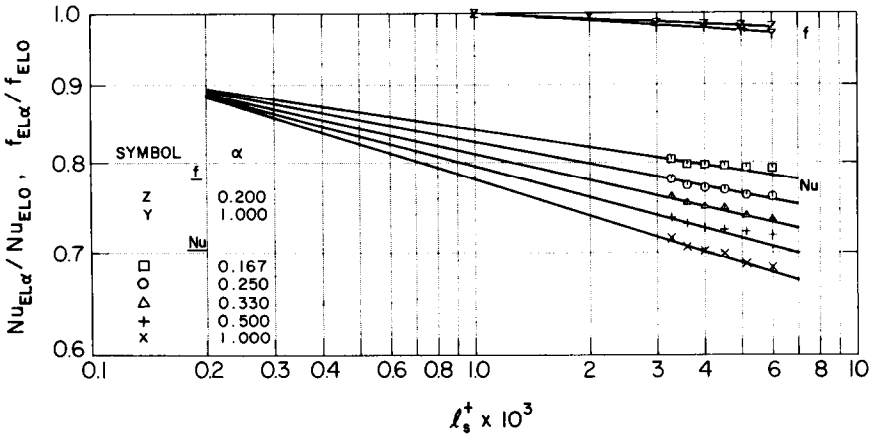

FIG. 6. Correction factors for finite aspect ratios.

Experimental data [23] for the same geometry show that C_D is approximately 2.0. However, qualitative justification can be provided for using C_D of the order of 0.8. Roshko [24] states that a blunt plate and a circular cylinder, oriented normal to the flow, are members of a basic family. The two geometries differ in their 'degree of bluffness'. For $Re_D > 1000$, $C_D = 1.0$ for a single circular cylinder. However, if one calculates the C_D on one cylinder in a staggered array with pitch/diameter = 3, one finds $C_D \cong 0.4$. So, C_D for the array of cylinders is only 40% of that for a single cylinder. Similarly, 40% of the C_D for flow normal to a thin plate is approximately 0.8. Additional confirmation for use of $C_D = 0.8$ was established in the development of a semi-empirical correlation for the friction factor of the offset strip-fin array [25]. Values of $0.7 < C_D < 0.9$ were tried, and $C_D = 0.8$ gave the best correlation. The present model uses $C_D = 0.8$ for the laminar and turbulent regimes.

Turbulent models

For $Re_b \geq Re_b^*$, a semi-empirical approach is used to calculate Nu_p and f_p.

Correlations for Nu_p and f_p. One may express equation (14) in terms of the heat transfer j-factors ($j \equiv Nu/RePr^{1/3}$) and solve it for ηj_p

$$\eta_f j_p = \frac{(1+\alpha+\delta)^2}{(1+\alpha)(1-\gamma)} \frac{Re_D}{Re_s} \eta j - \frac{(1+\alpha)\alpha}{1+\delta} \frac{Re_{sh}}{Re_s} j_e. \quad (30)$$

Equation (19) solved for f_p gives

$$f_p = \frac{(1+\alpha+\delta)(1+\gamma)}{1-\gamma} f - \alpha f_e - \frac{C_D t}{2l}. \quad (31)$$

For each of the surfaces of Table 1, six data points are selected such that $Re_b > Re_b^*$, where Re_b^* is calculated from equation (4). The reported j and f values are substituted in equations (30) and (31). The values j_e and f_e are calculated using equations for fully developed turbulent flow in a rectangular channel

$$Nu_e = 0.023(Re_{sh})^{0.8} Pr^{0.4} \quad (32)$$

$$f_e = 0.079(Re_{sh})^{-0.25}. \quad (33)$$

Thus, from equations (30) and (31) six values of j_p and f_p are obtained for each of the 21 surfaces. These are now correlated using multiple regression, with the Reynolds number Re_D, and the dimensionless geometric parameter l/D_h, as independent variables. The following equations were obtained

$$j_p = 0.36(Re_D)^{-0.433}(l/D_h)^{-0.174} \quad (34)$$

$$f_p = 15.33(Re_D)^{-0.785}(l/D_h)^{-0.324}. \quad (35)$$

Prediction of Nu_e and f_e. These values are calculated by equations (32) and (33). It is assumed that the fins do not affect the boundary layers on the top and bottom surfaces.

EXPERIMENTAL PROGRAM

The experimental portion of this study had two objectives:

(1) To take accurate friction factor data for precisely dimensioned offset strip-fin geometries.
(2) To conduct flow visualization experiments to study the flow on the fins and in their wakes, and observe the transition from laminar to turbulent flow.

Friction factor

A majority of the data available for the offset strip-fin were taken on industrially manufactured heat exchanger cores [1–6]. The possibility of burred fin edges results in a degree of uncertainty regarding the actual fin shape. Data available for scaled up arrays with precise dimensions [7, 8] do not include a systematic variation of the geometric parameters with values in the ranges of practical interest.

Eight models of the offset strip-fin were built for studying. Their dimensions are shown in Table 3. Data were also taken for one plain fin array.

The test sections were made with brass fins and plexiglass walls. The fins were made in the form of long brass plates with windows. These plates were placed in the slots made in the top and bottom walls, so that the

Table 3. Dimensions (mm) of test sections

Test-section	Symbol	l	t	s	D_h	δ	α	γ
Plain	●	762.0	0.813	4.267	7.669	0.001	0.123	0.191
1	□	25.4	0.406	4.674	7.518	0.016	0.123	0.087
2	○	12.7	0.406	4.674	7.518	0.032	0.123	0.087
3	△	25.4	0.813	4.267	6.096	0.032	0.112	0.191
4	◇	12.7	0.813	4.267	6.096	0.064	0.112	0.191
5	+	50.8	0.813	9.347	13.487	0.016	0.246	0.087
6	×	25.4	0.813	9.347	13.487	0.032	0.246	0.087
7	Z	12.7	0.813	9.347	13.487	0.064	0.246	0.087
8	Y	25.4	1.626	8.534	10.897	0.064	0.224	0.191

$h = 38.1$ for all test sections.
Symbols shown above are used in Figs. 9, 10 and 14.

windows in one plate were aligned with fins in the adjacent plate. The sides of all windows were filed by hand to ensure burr-free fin ends. The method of assembly is shown in Fig. 7. Figure 8 shows the completed test section with all the walls in place. The test sections were placed in the flow loop shown in Fig. 9. An entrance section is provided at the upstream end to allow a smooth transition from the circular piping.

Aqueous ethylene glycol (65–70% by weight) was used as the test fluid. One of two orifices measured the flow rates, controlled by the valves shown in Fig. 9. An inverted manometer, with a fluid of 1.75 specific gravity was used to measure the pressure drop across the orifices. The pressure drops across the test section (ΔP_1 and ΔP_2) were measured by an inclined manometer for heights smaller than 25 mm, and by a vertical manometer for larger heights. Fluid of specific gravity 0.75 was used in these manometers. The test sections had 15 fins in the flow direction, and five fins per row in the spanwise direction. ΔP_1 corresponds to the first eight fins of the test section, and ΔP_2 to the last seven fins where the flow is expected to be periodic fully developed.

The particular mixture of ethylene glycol that is chosen gives the desired Reynolds numbers for the flow rates available from the pump. Before running the tests, the densities and viscosities of various compositions were measured as functions of temperature. The properties were curve fitted to be used in data reduction. The temperature of the fluid was measured at the upstream end of the entrance section. An expansion tank was used to remove air from the system before taking data. The pressure drops ($\Delta P_1, \Delta P_2$) were converted to Fanning friction factors as follows

$$f = \frac{\Delta P D_h}{4L\frac{1}{2}\rho v^2} \tag{36}$$

where L is the length over which ΔP is measured. The velocity v corresponds to the minimum cross-sectional

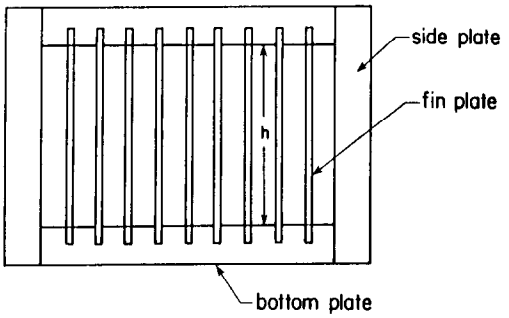

FIG. 8. Assembled test section.

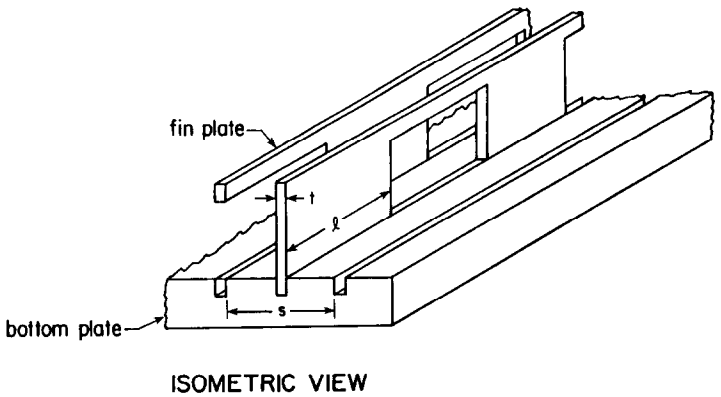

FIG. 7. Construction of test sections for f data.

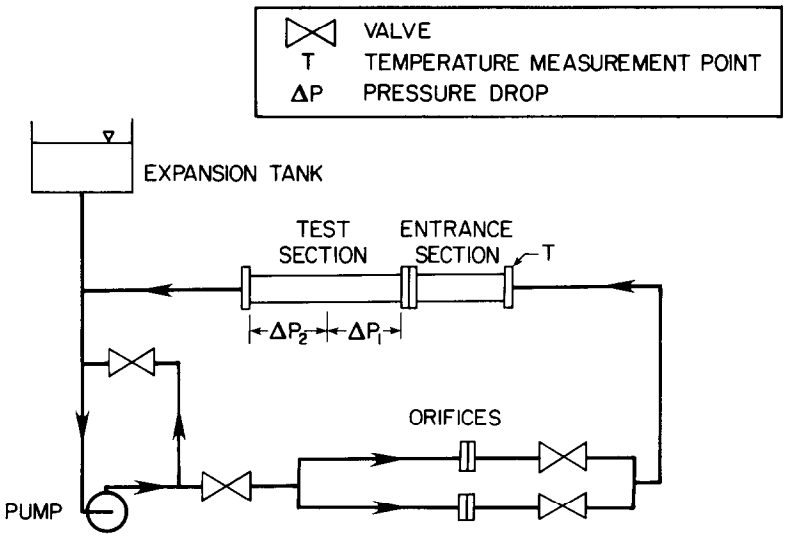

FIG. 9. Flow loop used for f data.

area in the test section

$$v = \frac{\dot{m}}{(s-t)h} \tag{37}$$

where $\dot{m}$ is the mass flow rate between two fin plates.

Results for the eight test sections and the plain fin are shown in Figs. 10 and 11. The symbols correspond to those in Table 3. These friction factors are based on the pressure drop ΔP_2. The friction factors in the developing region (ΔP_1) were found to be 5–8% higher than those based on ΔP_2. The plain fin data agree within 2% of the analytical solution of Curr *et al.* [27]. Figures 10 and 11 show that for the same aspect ratio, geometries with higher t/l have higher friction factors because of the contribution of the drag term $C_D t/2l$. As Re_D is increased, the relative contributions of f_p and f_e [equation (19)] decrease and the form drag begins to dominate, resulting in f being almost constant. This is evident for surfaces 3, 4, 7 and 8.

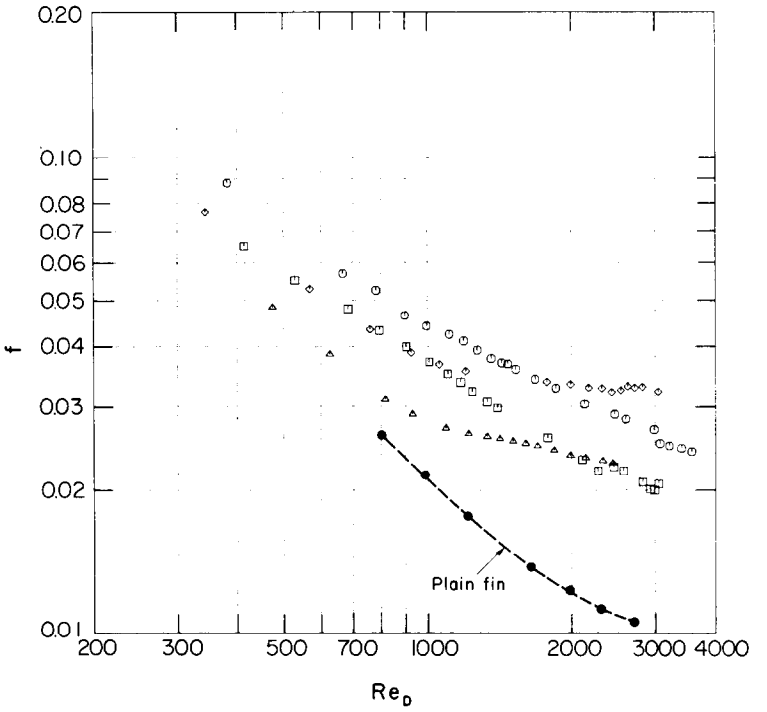

FIG. 10. f vs Re_D for four offset strip-fin test sections (1–4 in Table 3), and one plain fin. (Symbols are defined in Table 3.)

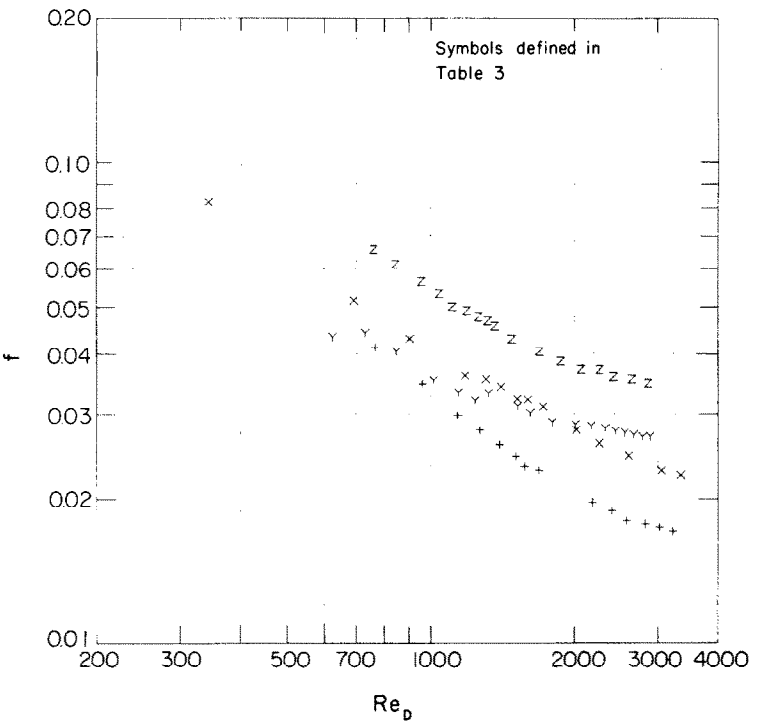

FIG. 11. f vs Re_D for four offset strip-fin test sections (5–8 in Table 3). (Symbols are defined in Table 3.)

Flow visualization

Visualization experiments were done on three scaled-up arrays. These arrays were made from plexiglass fins and a wooden base. Rectangular pieces of plexiglass were placed in slots cut into the base to form an offset strip-fin array. The method of assembly was similar to that used for the friction test sections, except that the fins were made individually, and that there is no top plate. The dimensions of the arrays are shown in Table 4. The top is left open to facilitate visualization. These arrays are placed in a water channel 305 mm wide and 4.6 m long. The wooden base fits in the channel leaving 3 mm gaps on either side. The arrays were composed of 20 fins in the flow direction and three fins per row in the spanwise direction. Black ink was used as the dye. It was introduced into the flow with a hypodermic needle at the end of a long vertical plastic tube. The needle was attached by a very thin tape to the downstream face of the fin whose wake was to be studied. This arrangement allowed introduction of the ink using gravity feed and without causing disturbances in the flow.

Table 4. Geometries of arrays used in flow visualization tests

No.	l	t	s	h	t/l
1	127.0	2.54	72.50	150.25	0.02
2	63.5	2.54	72.50	150.25	0.04
3	127.0	6.35	84.14	150.25	0.05

Results of the visualization experiments are shown in Fig. 12 and Table 5. Figure 12 shows that four distinct flow patterns may be observed as flow rate is increased. In Fig. 12(a) the wake is smooth and laminar. Figure 12(b) shows that oscillations first occur at the upstream of the second fin. These are carried to the upstream fin until, at a sufficiently high flow rate, vortices are shed. Table 5 shows three Reynolds numbers for each of the flow patterns observed. These values are for the 18th row of fins.

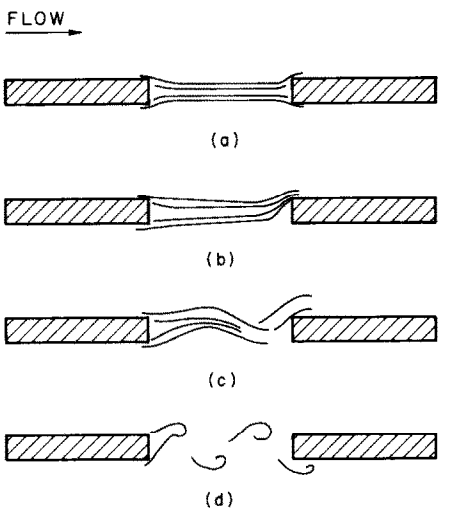

FIG. 12. Flow patterns observed in the visualization experiments.

Table 5. Reynolds numbers at the flow conditions of Fig. 12, for the three arrays of Table 4

Fig.		Array 1 $t/l = 0.02$	Array 2 $t/l = 0.04$	Array 3 $t/l = 0.05$
12(a)	Re_t	15	15	20
	Re_b	42	35	47
	Re_l	750	375	400
12(b)	Re_t	28	25	48
	Re_b	77	58	73
	Re_l	1400	625	960
12(c)	Re_t	58	62	107
	Re_b	130	116	168
	Re_l	2900	1550	2140
12(d)	Re_t	67	68	133
	Re_b	144	123	202
	Re_l	3350	1700	2660

Data taken for the second row of fins were found to be identical.

The three arrays of this experiment allow one to compare the effect of varying length and thickness. For arrays 1 and 2 (same t), a change in length does not affect the Re_t values. Re_b is smaller for array 2 because of smaller wake widths as defined by equation (2). For arrays 1 and 3 (same l), both Re_t and Re_b are higher while Re_l is lower, for the thicker plate.

Table 6. Comparison of equation (4) to flow visualization results

Array	Re_b^* equation (4)	Observed Re_b for Fig. 12(b) wake
1	43	42
2	22	35
3	59	47

The flow patterns observed in these experiments are to be related to the transition defined by equation (4). It is expected that the laminar models begin to underpredict the data when the wake becomes unstable. Thus, the changes of slopes of the f and j curves should correspond to the flow condition of Fig. 12(b) which shows the onset of oscillatory flow in the wakes. Application of equation (4) to the three arrays gives results that are shown in Table 6. The predicted values of Re_b^* are reasonably close to those observed for the flow pattern of Fig. 12(b). Equation (4) was developed by visually estimating the slope change points of 21 surfaces. Within the accuracy of these estimates, one may conclude that it predicts reasonably well the condition of the onset of oscillations in the wakes, and that this condition corresponds to the transition from laminar to turbulent flow as defined in Figs. 3 and 4.

PREDICTION OF j AND f VALUES

Heat transfer

Equation (14) is used to predict the j-factors for the 21 surfaces of Table 1. The ratio of the predicted j values (j_{pred}) to the reported j values (j_{exp}) with $\eta = \eta_f = 1$ is plotted vs the Reynolds number (Re_D) in Fig. 13. Equations (22), (24) and (26) are used for $Re_b \leqq Re_b^*$ (laminar range) and equations (32) and (34) are used for $Re_b > Re_b^*$ (turbulent range). Except for two surfaces the predictions are within $\pm 20\%$. The r.m.s. deviation of the ratios from the 1.0 line is 11.5%.

Friction factor

Equation (19) is used to predict the friction factors for the eight scaled up geometries of Table 3, and for the 21 heat exchangers of Table 1. For the laminar range ($Re_b \leqq Re_b^*$), equations (23), (25) and (27) are

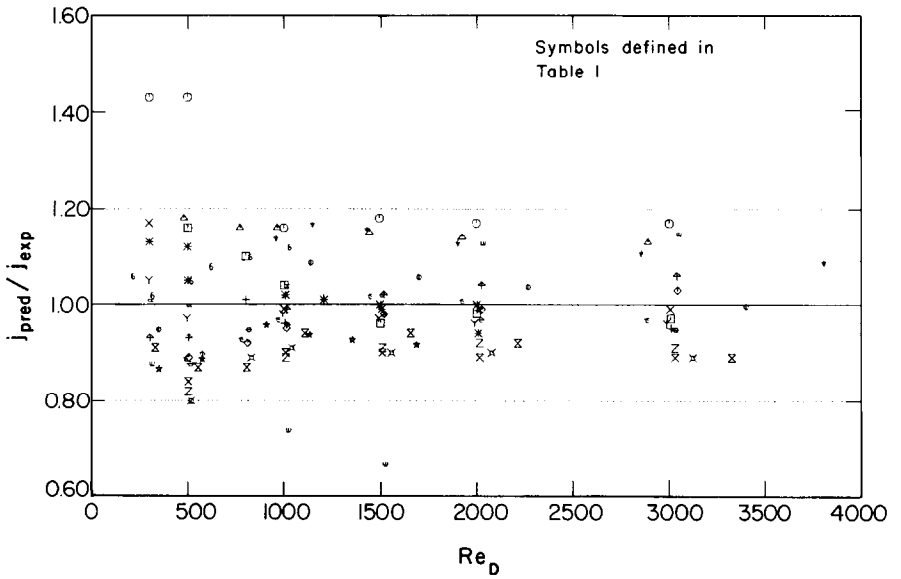

FIG. 13. Heat transfer predictions for the Table 1 data.

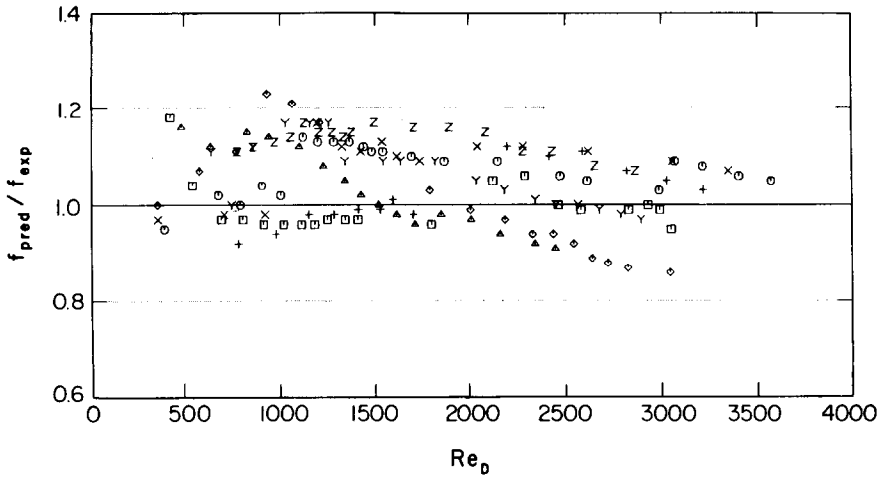

FIG. 14. Friction factor predictions for the Table 3 data.

used. For the turbulent range ($Re_b > Re_b^*$), equations (33) and (35) are used. The predictions are plotted as the ratio f_{pred}/f_{exp} vs Re_D.

Table 3 data. The predictions for the data of the present study are shown in Fig. 14. All predictions are within $\pm 20\%$ of the data. The r.m.s. deviation is 9.5%.

Equation (4), used to predict Re_b^*, was developed using the 21 heat exchanger cores of Table 1. Its ability to predict Re_b^* for the Table 3 geometries is examined in Table 7. Except for surface 7 the predicted Re_b^* values agree with the Re_b at the observed slope changes within $\pm 20\%$.

Heat exchanger data. Friction factor predictions for the 21 heat exchanger surfaces are shown in Fig. 15. The predictions are within $\pm 20\%$ of the data for 16 of the 21 surfaces. The r.m.s. deviation of all predictions is 16.8%. Examination of Fig. 15 shows a tendency to underpredict the friction factor. This would occur if burred fin edges existed in some of the cores.

Laminar model

If the laminar model for heat transfer is used to predict j over the entire Re_D range, it is expected that for $Re_b > Re_b^*$, the predictions will fall below the data.

A plot of the j predictions using the laminar equations (22), (24) and (26) is shown in Fig. 16. The ratio j_{pred}/j_{exp} is plotted vs the entrance length parameter l_s^+ used in equation (22). At approximately $l_s^+ = 0.0012$, the predictions start to fall below the data, with increasing deviation as l_s^+ is decreased (Re_D is increased). This figure clearly shows that a laminar model should not be used for $Re_b > Re_b^*$ as defined by equation (4).

PRACTICAL CONCERNS

Effect of burrs and roughness

Comparison of Figs. 1, 5 and 7 shows that the unit cell and the model test sections are idealizations of the actual geometry. There are two major differences: (1) the fin ends in an actual core may be burred; and (2) there is a roughness on the top and bottom walls of the actual surface. If these two factors significantly affect the heat and momentum transfer, it would be more evident in the turbulent than in the laminar regime. An assessment of the burr and roughness effect on the friction factor was made for the turbulent regime as follows. Burrs and roughness do not exist for the Table 3 geometries. The same method used to develop equation (35) was applied to the Table 3 turbulent regime data. The resulting equation is

$$f_p = 3.78 Re_D^{-0.62} (l/D_h)^{-0.23}. \quad (38)$$

Table 7. Comparison of equation (4) to Table 3 data

Surface	Re_D at slope change	Re_b at slope change	Re_b^* equation (4)	Re_b^*/Re_b
1	2000	211	188	0.89
2	1400	140	119	0.85
3	1300	271	313	1.15
4	1000	197	199	1.01
5	1900	221	188	0.85
6	1400	148	119	0.80
7	1500	140	76	0.54
8	1100	231	200	0.87

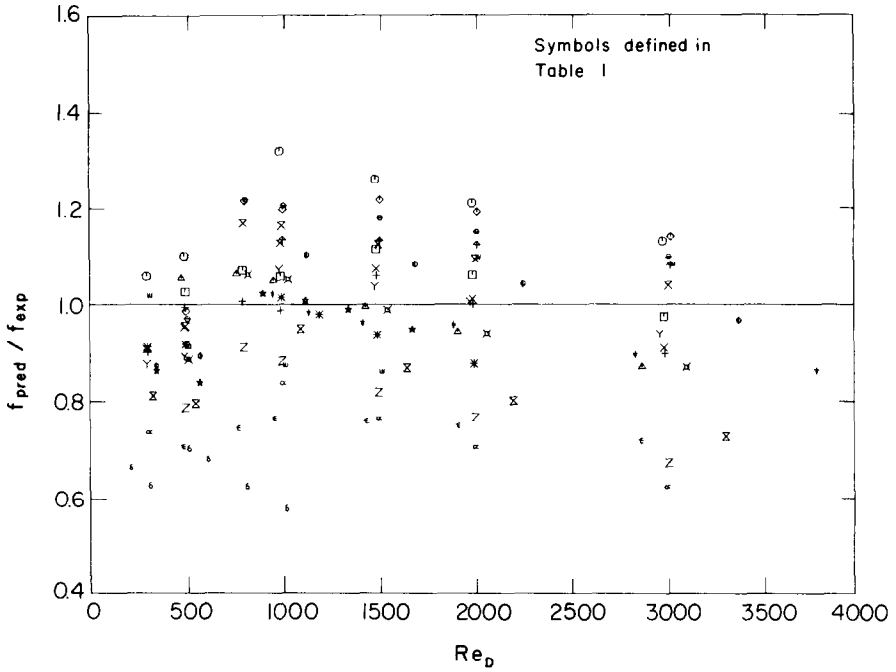

FIG. 15. Friction factor predictions for the Table 1 data.

Using equations (33) and (38) to predict f_p for the turbulent regime of the Table 1 geometries, a plot of f_{pred}/f_{exp} was made (Fig. 7). One is interested in determining whether there is a significant underprediction on Fig. 17, as compared to Fig. 15. A comparison of corresponding points on Figs. 17 and 15 show 9–20% underprediction at the low Re_D end and 0–8% underprediction at the highest values of Re_D. There is no obvious reason why the underprediction would be greater at the lower Re_D values. Hence, it appears that the combined effect of burrs and roughness on the friction factor may be, on the average 4–14% in the turbulent regime.

In the case of heat transfer, the roughness should cause an enhancement, whereas burred fin ends may cause leading edge separation, and a decrease in the heat transfer. These two effects tend to cancel. If only the roughness is present, the surface may show a small enhancement. Typically, a 50% increase in the heat transfer coefficient on the top and bottom walls would

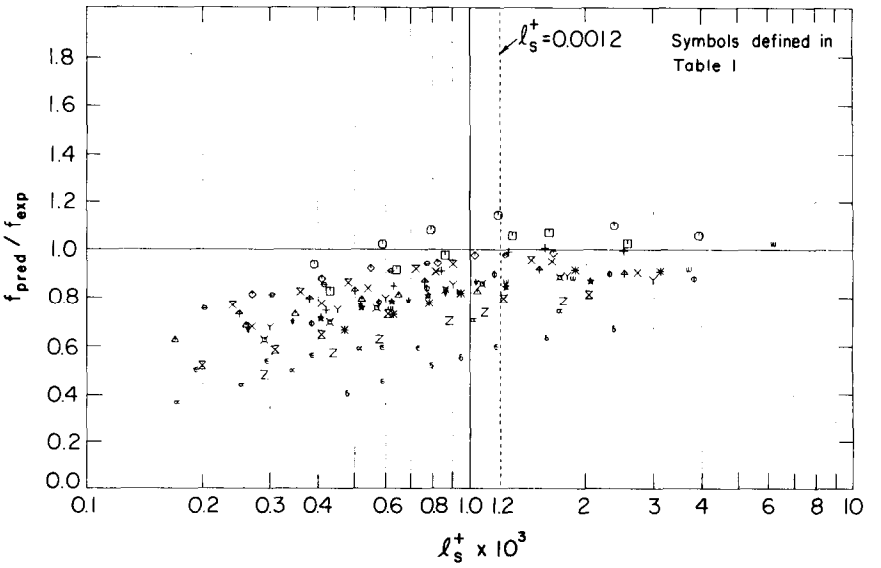

FIG. 16. Heat transfer predictions using the laminar model for the Table 1 data.

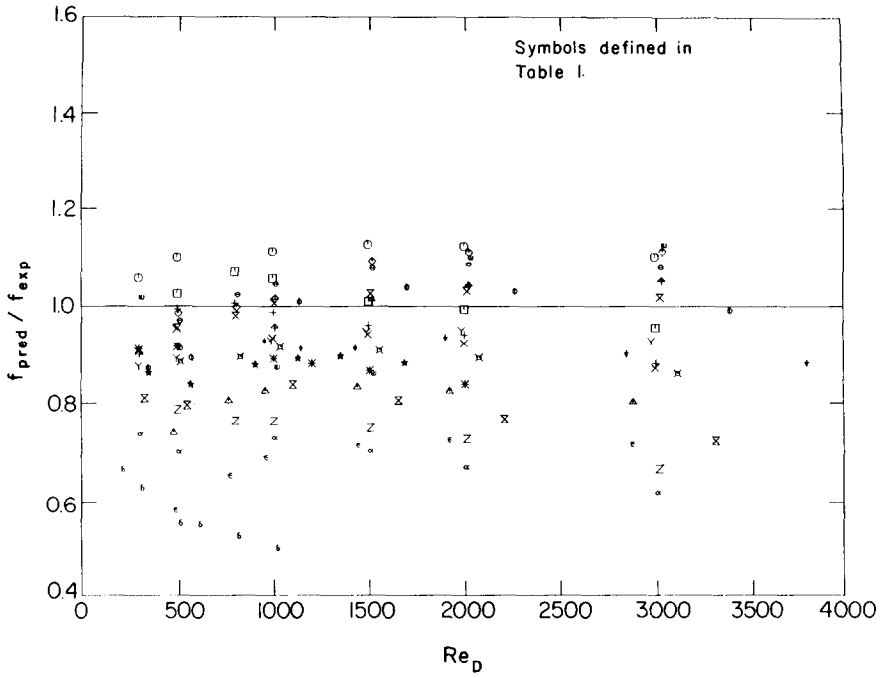

FIG. 17. Friction factor predictions using equation (38) for the Table 1 data.

result in a 2–5% increase of the composite heat transfer coefficient (h_o).

Whether burrs existed on the surfaces of Table 1, and the size of such burrs is unknown [28]. This represents an uncertainty in the data of these surfaces.

Empirical correlations

Empirical curve fits of the data are easier to use than the models described above and may be preferred by the industrial designer. The empirical j and f correlations of Wieting [15] were previously mentioned. He chose $Re_D < 1000$ for his laminar correlation and $Re_D > 2000$ for the turbulent correlation. The reduced data use the D_h definition of Kays and London [3] as described in the Appendix. In the present study similar correlations were developed using the Table 1 data and the criterion for Re_6^* [equation (4)] as the limit on the laminar correlations. Thus, for $Re_D \leqq Re_D^*$ (Re_D^* corresponds to Re_6^*), the laminar equations are used. Because of the uncertainty in reading the j and f plots for the 21 surfaces, the lower limit on the turbulent equations was chosen as $Re_D^* + 1000$. The following equations were obtained.

Laminar range ($Re_D \leqq Re_D^*$):

$$f = 8.12(Re_D)^{-0.74}(l/D_h)^{-0.41}(\alpha)^{-0.02} \quad (39)$$

$$j = 0.53(Re_D)^{-0.50}(l/D_h)^{-0.15}(\alpha)^{-0.14}. \quad (40)$$

Turbulent range ($Re_D \geqq Re_D^* + 1000$):

$$f = 1.12(Re_D)^{-0.36}(l/D_h)^{-0.65}(t/D_h)^{0.17} \quad (41)$$

$$j = 0.21(Re_D)^{-0.40}(l/D_h)^{-0.24}(t/D_h)^{0.02}. \quad (42)$$

The r.m.s. deviations are 8.7%, 8.6%, 13.1% and 8.1%, respectively. The correlations predict 80% of the f data and 75% of the j data within $\pm 10\%$ for the laminar regime, and 88% of the f data and 97% of the j data are predicted within $\pm 20\%$ for the turbulent regime.

Overall 82% of the f data and 91% of the j data are correlated within $\pm 15\%$. The Wieting correlations predict 85% of the data within $\pm 15\%$ for both f and j.

CONCLUSIONS

1. An equation was developed to predict the transition from laminar to turbulent flow in the offset strip channel. Flow visualization experiments showed that the transition occurs at the onset of oscillating velocities in the wake.
2. Analytical models were developed to predict the heat transfer coefficient and the friction factor in the offset strip-fin. For the laminar region the model is based on a numerical solution done by Sparrow and Liu [18], and a semi-empirical method was used for the turbulent region. The r.m.s. deviation of the predictions of the heat transfer model for data of 21 heat exchangers is 11.5%, and that of the friction model is 16.8%.
3. Friction factor data were taken on eight scaled-up, idealized geometries. The friction model predicted these data with an r.m.s. deviation of 9.5%.
4. Flow visualization experiments were done to study the flow in the fin wakes and its effect on transition. Three geometries were tested. Flow patterns in the

wake may be correlated by using a wake width based Reynolds number.

5. Empirical correlations were developed to calculate the heat transfer coefficient and friction factor. These correlations are based on a different definition for hydraulic diameter than that used in the correlations of Wieting [15], because the area of the fin ends has been included. Overall, 82% of the f data and 91% of the j data are correlated within $\pm 15\%$. The change from laminar to turbulent equations is based on the equation developed to determine transition.

Acknowledgement—This work was performed under Department of Energy contract DE-AS02-79ER10394.

REFERENCES

1. U. T. Joyner, Experimental investigation of entrance region heat transfer coefficients, NACA ARR 3K01 (1943).
2. R. H. Norris and W. A. Spofford, High performance fins for heat transfer, *Trans. Am. Soc. mech. Engrs* **64**, 489–496 (1942).
3. W. M. Kays and A. L. London, *Compact Heat Exchangers*, 3rd edn. McGraw-Hill, New York (1984).
4. F. M. Walters, Data Item No. 63.02, AiResearch Manufacturing Co., Document No. AP-69-5348 (August 1969).
5. A. L. London and R. K. Shah, Offset rectangular plate-fin surfaces—heat transfer and flow friction characteristics, *J. Engng Pwr* **90**, 218–228 (1968).
6. S. Mochizuki and Y. Yagi, Heat transfer and friction characteristics of strip-fins, *Heat Transfer—Japan. Res.* **6**, 36–59 (1977).
7. E. M. Sparrow and A. Hajiloo, Measurement of heat transfer and pressure drop for an array of staggered plates aligned parallel to an air flow, *J. Heat Transfer* **102**, 426–432 (1980).
8. R. S. Mullisen and R. I. Loehrke, Enhanced heat transfer in parallel plate arrays, *21st National Heat Transfer Conference*, Seattle, WA (July 1983).
9. D. B. Adarkar and W. M. Kays, Heat transfer in wakes, TR No. 55, Department of Mechanical Engineering, Stanford University (April 1963).
10. R. I. Loehrke, R. E. Roadman and G. W. Read, Low Reynolds number flow in plate wakes, ASME Paper No. 76-WA/HT-30 (December 1976).
11. R. I. Loehrke, J. C. Lane and R. L. Zelenka, Heat transfer from interrupted plate surfaces, TR HT-pp791, Department of Mechanical Engineering, Colorado State University (November 1979).
12. S. Mochizuki and Y. Yagi, Characteristics of vortex shedding in plate arrays, *Flow Visualization II, Proc. 2nd Int. Symposium on Flow Visualization*, Bochum, W. Germany, pp. 99–103 (1980).
13. W. M. Kays, Compact heat exchangers. In *AGARD Lecture Series No. 57 on Heat Exchangers* (Edited by J. J. Ginoux), AGARD-LS-57-72 (1972).
14. S. V. Manson, Correlations of heat transfer data and of friction data for interrupted plane fins staggered in successive rows, NACA Technical Note 2237 (December 1950).
15. A. R. Wieting, Empirical correlations for heat transfer and flow friction characteristics of rectangular offset-fin plate-fin heat exchangers, *J. Heat Transfer* **97**, 488–490 (1975).
16. H. Usami, Private communication, Fuji Heavy Industries Ltd., Tochigi, Japan (July 1983).
17. E. M. Sparrow, B. R. Baliga and S. V. Patankar, Heat transfer and fluid flow analysis of interrupted wall channels with application to heat exchangers, *J. Heat Transfer* **99**, 4–11 (1977).
18. E. M. Sparrow and C. H. Liu, Heat-transfer, pressure-drop, and performance relationships for in-line, staggered, and continuous plate heat exchangers, *Int. J. Heat Mass Transfer* **22**, 1613–1625 (1979).
19. S. V. Patankar and C. Prakash, An analysis of the effect of plate thickness on laminar flow and heat transfer in interrupted-plate passages, *Int. J. Heat Mass Transfer* **24**, 1801–1810 (1981).
20. R. K. Shah and R. L. Webb, Compact and enhanced heat exchangers. In *Heat Exchangers Theory and Practice* (Edited by J. Taborek *et al.*), pp. 440–441. Hemisphere, Washington (1983).
21. R. K. Shah and A. L. London, *Laminar Flow Forced Convection in Ducts*. Academic Press, New York (1978).
22. L. M. Milne-Thomson, *Theoretical Hydrodynamics*, 4th edn, p. 319. Macmillan, New York (1960).
23. S. F. Hoerner, *Fluid Dynamic Drag*, pp. 3–16. Published by the author, Midland Park, NJ (1965).
24. A. Roshko, On the wake and drag of bluff bodies, *J. aeronaut. Sci.* **22**, 124–132 (1955).
25. R. L. Webb and H. M. Joshi, Prediction of the friction factor for the offset strip-fin matrix, *Proc. ASME-JSME Thermal Engineering Joint Conference*, ASME, New York, Vol. 1, pp. 1801–1810 (1983).
26. S. W. Churchill and R. Usagi, A general expression for the correlation of rates of transfer and other phenomena, *A.I.Ch.E. Jl* **18**, 1121–1128 (1972).
27. R. M. Curr, D. Sharma and D. G. Tatchell, Numerical predictions of some three dimensional boundary layers in ducts. In *Computational Methods in Applied Mechanical Engineering*, Vol. 1, pp. 143–158 (1972).
28. R. K. Shah, Private communication, Harrison Radiator, Lockport, NY (October 1984).

APPENDIX

The j, f and Re_D values in Table 1 were calculated using D_h and Re defined by equations (7) and (8), respectively. This D_h definition uses the actual heat transfer surface area (A) (which includes the blunt fin faces), and the true minimum flow area $[A_c = (s-t)h]$. Using equation (6) for D_h, the $Re_D = D_h v/\nu$. The references for the Table 1 data used different definitions for A and/or A_c, which affects the definition of D_h and Re. References [3–5] define $A_c = sh$. References [3,5] (surfaces 1–16 and 18–20) use the same A as in the present work. Reference [4] (surfaces 17, 21) neglects the area of the blunt fin faces. The data presented in refs. [3–5] were adjusted to use the D_h and Re definitions of equations (7) and (8), respectively.

TRANSFERT DE CHALEUR ET FROTTEMENT DANS UN EXCHANGEUR DE CHALEUR A BANDE-AILETTE OFFSET

Résumé—On présente des modèles analytiques pour estimer le coefficient de transfert thermique et le coefficient de frottement d'une surface d'échangeur de chaleur avec bande-ailette offset. On considère les deux régimes d'écoulement laminaire et turbulent. Basée sur les conditions dans le sillage, une équation est établie pour prédire la transition entre laminaire et turbulent. Des visualisations d'écoulement sont conduites pour identifier la structure de l'écoulement à la transition. La condition prédite par l'équation correspond à l'apparition de vitesses oscillantes dans les sillages de l'ailette. Des équations sont obtenues pour le nombre de Nusselt et pour le coefficient de frottement en écrivant les bilans d'énergie et de quantité de mouvement sur une cellule unitaire de la géométrie considérée. On utilise une solution numérique pour calculer Nu et f sur les ailettes dans le régime laminaire, et on utilise une approche semi-empirique pour le régime turbulent. Des résultats de calcul sont comparés aux données expérimentales prises dans la présente étude et aussi pour des échangeurs de chaleur réels. Les modèles prédisent toutes les données à mieux que $\pm 20\%$.

WÄRMEÜBERGANG UND DRUCKABFALL IN EINEM WÄRMEAUSTAUSCHER MIT VERSETZTEN, STREIFENFÖRMIGEN RIPPEN

Zusammenfassung—Die Abhandlung stellt ein analytisches Modell zur Bestimmung des Wärmeübergangs-Koeffizienten und des Widerstandsbeiwertes eines Wärmetauschers mit versetzten, streifenförmigen Rippen vor. Es werden zwei Strömungsarten, laminar und turbulent, unterschieden. Aufbauend auf den Verhältnissen im Nachlauf der Rippen wird eine Gleichung entwickelt, um den Übergang von laminarer in turbulente Strömung zu bestimmen. Es werden Experimente zur Sichtbarmachung der Strömung durchgeführt, um die Strömungsstruktur beim Übergang zu bestimmen. Die mit der Gleichung für den Übergang ermittelte Bedingung stimmt mit dem Auftreten von Geschwindigkeits-Oszillationen in der Wirbelschleppe überein. Es werden Gleichungen für die Nusselt-Zahl und den Widerstandsbeiwert durch Erstellen von Energie- und Impuls-Bilanzen an einer Elementarzelle der versetzten Rippengeometrie aufgestellt. Im laminaren Bereich wird für die Berechnung von Nu und f eine numerische Lösung, im turbulenten Bereich eine halbempirische Näherung angewandt. Die Berechnungen werden mit Messungen an vergrößerten Objekten, welche in der vorliegenden Arbeit durchgeführt wurden, und mit Messungen an Wärmetauschern der praktischen Anwendung verglichen. Der relative Fehler war stets kleiner als $\pm 20\%$.

ТЕПЛОПЕРЕНОС И ТРЕНИЕ В ТЕПЛООБМЕННИКЕ СО СМЕЩЕННЫМИ ПЛАСТИНЧАТЫМИ РЕБРАМИ

Аннотация—Предложены аналитические модели для расчета коэффициентов теплопереноса и трения на поверхности теплообменника со смещенными пластинчатыми ребрами. Установлено наличие двух режимов течения: ламинарного и турбулентного. С использованием условий в следе выведено уравнение для расчета перехода от ламинарного к турбулентному течению. Выполнены эксперименты по визуализации течения для определения структуры переходного режима потока. Условие, рассчитанное по уравнению перехода, соответствует условию возникновения пульсаций скорости в следе ребра. Получены уравнения для расчета значений числа Нуссельта и коэффициента трения из балансов энергии и количества движения, записанных для элементарной ячейки конфигурации со смещенными пластинчатыми ребрами. Для расчета Nu и f при ламинарном обтекании ребер используется численное решение, а при турбулентном обтекании-полуэмпирический подход. Результаты расчета сравниваются с данными, полученными в этой же работе для конфигураций увеличенного масштаба, и с данными для обычных теплообменников. Точность расчета по моделям лежит в пределах $\pm 20\%$.